

Excitonic effects in absorption and emission of 2D group-III nitrides

M.S. Prete, D. Grassano,* and O. Pulci

*Department of Physics, and INFN, University of Rome Tor Vergata,
Via della Ricerca Scientifica 1, I-00133 Rome, Italy*

Ihor Kupchak

*V.E. Lashkaryov Institute of Semiconductor Physics,
National Academy of Sciences of Ukraine, Kyiv, Ukraine*

Friedhelm Bechstedt

*Institut für Festkörperteorie und -optik, Friedrich Schiller Universität, Max-Wien-Platz 1, 07743 Jena, Germany
(Dated: December 15, 2024)*

Spatial confinement effects and reduced screening play a dramatic role in two-dimensional systems and offer extra routes to control their optical properties. We present a systematic *ab-initio* study of the exciton behavior in semiconducting monolayer nitride compounds BN, AlN, GaN, and InN. We calculate the optical spectra for in-plane and out-of-plane light polarization by solving the Bethe-Salpeter equation, i.e., including quasiparticle and excitonic effects. The properties of bound band-edge excitons such as binding energies and localization radii are compared with predictions of an analytical model for excitons in two dimensions. Our calculations reveal strong excitonic effects due to the interplay of low dimensionality, confinement effects, and reduced screening. In addition, we find exciton radiative lifetimes ranging from tenths of picoseconds (BN) to tenths of nanoseconds (InN) at room temperature, thus making 2D nitrides, especially InN, most promising materials for light-emitting diodes and high-performance solar cells.

I. INTRODUCTION

Since the discovery of graphene, the research on alternative two-dimensional (2D) materials has gained enormous interest. Silicene, germanene, phosphorene, and transition metal dichalcogenides are just a few examples of classes of novel low-dimensional systems, which may serve as building blocks for efficient nanoelectronic and nanooptical devices [1–4]. On the other hand, bulk group-III nitrides such as GaN, AlN and InN are most important materials for solid state lighting, as witnessed by the Nobel prize awarded in 2014 to Akasaki, Amano and Nakamura [5]. The possibility to play with dimensionality to enhance the already exceptional properties of bulk nitrides, has caused an avalanche of attempts to grow 2D nitrides, although the strong tendency for sp^3 bonding makes their preparation extremely difficult. Only monolayer BN can, in principle, be easily prepared by exfoliation from hexagonal bulk BN [6]. Promising experimental attempts to obtain 2D AlN and GaN have recently appeared [7, 8]. Measurements of GaN sheets encapsulated in graphene seem to suggest a fundamental optical gap of about 5 eV [9]. These successful experiments pave the way to new photovoltaic and optical nanodevices based on 2D nitrides [10].

The recent progress in achieving growth of ultrathin 2D AlN and GaN layers on certain substrates as well as the exfoliation of BN monolayers suggests the possibility to also prepare 2D InN. Therefore, a theoretical

understanding of the monolayer properties of BN, AlN, GaN, and InN, in particular of their optical absorption and emission properties, may push forward the experimental activities on 2D nitrides. Several studies have been focused on the tunable electronic gap [11–14]. Excitonic properties have been recently investigated for GaN [15, 16] and InN [17, 18], in addition to the activities on the well-known BN layer [19].

In this paper, we tackle this goal through a systematic *ab-initio* study of the optical properties of 2D group-III nitrides BN, AlN, GaN, and InN. We focus on the absorption and emission spectra near the onsets for in- and out-of-plane light polarization. The dominating bound excitons are studied in detail, in particular the influence of spatial confinement effects and reduced screening of the electron-hole interaction. For the exciton ground state we calculate the binding energy and the excitonic radius and compare the results with those of model calculations. The emission is characterized by the excitonic radiative lifetime. The paper is organized as follows: in Sec. II we describe the computational and theoretical *ab-initio* methods employed. Then, in Sec. III, we present and discuss results on optical spectra and radiative lifetimes of the 2D materials. Finally, in Sec. IV we draw conclusions.

II. COMPUTATIONAL METHODS

A. Ground and excited states

Our *ab-initio* calculations of the structural and electronic properties proceed in three steps: first, we calcu-

* davide.grassano@roma2.infn.it

late the equilibrium geometry of 2D honeycomb sheets within density-functional theory (DFT) [20] as implemented in the *Quantum Espresso* code [21, 22], using the local density approximation (LDA) to describe exchange and correlation (XC). Minimizing the total energy with respect to the atomic coordinates the lattice constant and other geometry parameters are derived. The isolated 2D crystals are modeled within a supercell with a vacuum layer of thickness L of about 15 Å between the periodic images.

Second, the single-quasiparticle excitation energies are derived by correcting the Kohn-Sham (KS) eigenvalues $\varepsilon_{n\mathbf{k}}^{KS}$ of the DFT [20]. We accurately determine the electronic levels by solving the quasiparticle (QP) equation within the G_0W_0 approximation for the electronic self-energy [23] as implemented in the *chisig* code [24]. The QP equation for Bloch states $\psi_{n\mathbf{k}}^{QP}$

$$(T + V_{ext} + V_H + \Sigma)\psi_{n\mathbf{k}}^{QP} = \varepsilon_{n\mathbf{k}}^{QP}\psi_{n\mathbf{k}}^{QP} \quad (1)$$

with kinetic energy T , the electron-ion potential V_{ext} , the Hartree potential V_H , and the XC self-energy $\Sigma = \Sigma_X + \Sigma_C$ is solved using first order perturbation theory with respect to the perturbation $\Sigma - V_{XC}$ of the KS system, with V_{XC} as the XC potential. For the exchange part of the self-energy Σ_X , we use a $102 \times 102 \times 1$ \mathbf{k} -point mesh centered on Γ in the BZ. For the correlation part of the self-energy Σ_C and for the screened Coulomb interaction W , we use a $51 \times 51 \times 1$ \mathbf{k} -point mesh and 300 bands.

B. Electron-hole-pair states

In the third step, we account for the electron-hole interaction, calculating the screened electron-hole attraction and the unscreened electron-hole exchange. We construct the corresponding electron-hole pair Hamiltonian H_{exc} and solve the homogeneous Bethe-Salpeter equation (BSE) [23]

$$H_{exc}|S\mathbf{Q}\rangle = E_S(\mathbf{Q})|S\mathbf{Q}\rangle. \quad (2)$$

Applying the *dp4exc* code [25] the eigenstates $|S\mathbf{Q}\rangle$ with set of quantum numbers S , translational momentum $\hbar\mathbf{Q}$, and energy $E_S(\mathbf{Q})$ are determined within the Tamm-Dancoff approximation. Thereby, not only in the QP equation (1) but also in the BSE (2), we cut the Coulomb interactions between the sheet crystals in normal direction.

For a better understanding of the lowest-energy ground state excitons with $S = 0$, $\mathbf{Q} = 0$ and excitation energy $E_0(0)$ with an approximate 1s character, we compare the *ab-initio* results for the exciton binding energy E_b and the exciton radius r_{exc} obtained within the accurate, but computationally heavy BSE calculations, with predictions of an analytical model of excitons in two dimensions [26, 27]. Thereby, we focus on the bound excitons at the absorption edge. The Schrödinger equation, with

excitonic eigenvalues E_n and eigenfunctions $\phi_n(\boldsymbol{\rho})$, can be formulated with an effective Hamiltonian as [27]

$$\left\{ E_g - \frac{\hbar^2}{2\mu} \nabla_{\boldsymbol{\rho}}^2 + W(\boldsymbol{\rho}) \right\} \phi_n(\boldsymbol{\rho}) = E_n \phi_n(\boldsymbol{\rho}), \quad (3)$$

where the reduced exciton mass $\mu = m_e m_h / (m_e + m_h)$ is introduced within the effective mass approximation (EMA) with the electron (hole) mass m_e (m_h) derived from dispersion of the lowest conduction (highest valence) band. The relative distance between electron and hole is described by the vector $\boldsymbol{\rho}$. The screened Coulomb interaction is [27–29]

$$W(\boldsymbol{\rho}) = -\frac{e^2}{4\alpha_{2D}} \left[H_0\left(\frac{\rho}{2\pi\alpha_{2D}}\right) - Y_0\left(\frac{\rho}{2\pi\alpha_{2D}}\right) \right], \quad (4)$$

with H_0 and N_0 as the Struve and Neumann functions, respectively. $\alpha_{2D} = L \cdot (\text{Re}\epsilon_{\parallel}(\omega = 0) - 1)/4\pi$ denotes the 2D static electronic polarizability of the sheet, which is computed from the in-plane dielectric function ϵ_{\parallel} in the limit of vanishing wave vector and frequency.

C. Optical properties

With the solutions $|S\mathbf{Q}\rangle$ and $E_S(\mathbf{Q})$ of the BSE (2), the frequency-dependent dielectric tensor $\epsilon_{\parallel/\perp}(\omega)$ can be directly computed for light polarization parallel/perpendicular to the crystal sheets in the superlattice arrangement. Thereby, because of the neglect of photon wave vector, only vertical optical transitions appear with $\mathbf{Q} = 0$ and optical transition matrix elements $\langle c\mathbf{k}|p_{\parallel/\perp}|v\mathbf{k}\rangle$ of the momentum operator between KS valence ($|v\mathbf{k}\rangle$) and conduction ($|c\mathbf{k}\rangle$) states. The optical properties of isolated sheet crystals are described by the optical conductivities $\sigma_{\parallel/\perp}(\omega)$, which are independent of the vertical distance L between the sheets [30]. Their real (imaginary) parts describe the absorption (dielectric) properties for in- and out-of-plane light polarization.

Following Moody *et al* [31], we calculate the radiative decay rate $\gamma_S(0)$ and lifetime $\tau_S(0)$ of an exciton in state S with vanishing wavevector $\mathbf{Q} = 0$ as [32]

$$\gamma_S(0) = \tau_S^{-1}(0) = \frac{8\pi e^2 E_S(0)}{\hbar^2 c} \frac{\mu_S^2}{A_{uc}}, \quad (5)$$

where μ_S^2 is the square modulus of the exciton dipole transition matrix element divided by the number of \mathbf{k} -points employed in the calculation. A_{uc} is the area of the unit cell and $E_S(0)$ is the exciton excitation energy. To compute the thermal average radiative lifetimes $\langle \tau_S \rangle$ of excitons in excitonic bands $E_S(\mathbf{Q})$ at temperature T we apply the formula obtained in the classical high-temperature limit [32]

$$\langle \tau_S \rangle = \tau_S(0) \frac{3}{4} \left(\frac{E_S^2(0)}{2Mc^2} \right)^{-1} k_B T \quad (6)$$

with $M = m_e + m_h$ being the translational (total) mass of the exciton.

III. RESULTS AND DISCUSSION

A. Geometry and electronic properties

Two-dimensional sheets of group-III nitrides have as equilibrium geometry a flat honeycomb structure similar to graphene [33] but with reduced D_{3h} symmetry. As in graphene and BN, also in AlN, GaN and InN the first-row element N tends toward a sp^2 hybridization and in-plane III-N bonds. Therefore, the geometries are only characterized by the lattice constant a . The absence of buckling is due to the presence of nitrogen, that possesses an atomic radius small enough to support strong sp^2 hybridization. The lattice parameters listed in Table I, follow a clear chemical trend with increasing atomic number of the cation. The lattice constants are smaller than those for the 3D bulk counterparts, consistently with the sp^2 bonding being stronger than the sp^3 one.

	a (Å)	E_g (eV)
BN	2.48	7.2 (KK)/6.7 (K Γ)
AlN	3.03 (exp: 3.13)	6.5 ($\Gamma\Gamma$)/5.8 (K Γ)
GaN	3.15	4.5 ($\Gamma\Gamma$)/4.6 (K Γ)
InN	3.52	1.7($\Gamma\Gamma$)/2.1 (K Γ)

TABLE I. Lattice constant a and direct and indirect quasi-particle gaps E_g calculated within the G_0W_0 for 2D nitrides. The band edge positions in the BZ are indicated in parenthesis. For AlN an experimental lattice parameter is given [7].

For what concerns the electronic properties, it is well known that 2D III-N monolayers, conversely to graphene, do not show any Dirac cone in the electronic band structure [13–15, 33]. The band structures, see Supplemental Material (SM) Fig. SM1, are characterized by indirect gaps with the valence band maximum (VBM) at K and the conduction band minimum (CBM) at Γ . Apart from BN with a lowest direct band gap at K , the other nitrides exhibit a direct gap at Γ . While BN and AlN tend to be indirect semiconductors, GaN and InN are direct 2D crystals [13]. Other G_0W_0 computations observe an indirect gap also for GaN [15]. Table I indicates that the valence band maxima at Γ and K are not far away from each other. The gap E_g , listed in Table I can be understood as due to the presence of two different kind of atoms, bearing different electronegativity, in the two hexagonal sublattices. A charge transfer occurs from the cation (B, Al, Ga, In) to the anion (N) with a subsequent opening of the electronic QP gaps, which span from about 7 eV for 2D BN to 1.7 eV for 2D InN, respecting the chemical trend. The electronic gaps shown by 2D III-N monolayers are much larger than those of their 3D bulk counterparts (see collections in [11, 19, 34]), as illustrated in Fig. 1. Quantum confinement of the electrons is the main responsible for this behavior. Moreover, the reduced 2D screening also modifies the QP corrections.

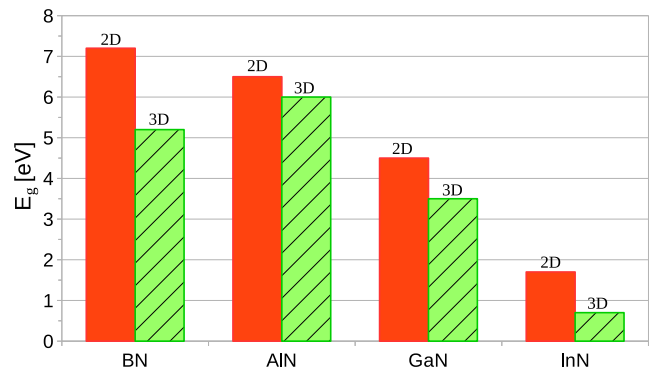


FIG. 1. Comparison between the electronic QP gaps in 2D sheets and 3D bulk materials.

B. Excitonic effects in optical spectra

For all 2D nitride sheets we have calculated and compared the dynamical optical conductivities $\sigma_{\parallel/\perp}(\omega)$ for in-plane/out-of-plane light polarization at three different level of approximations: within the independent-particle approximation (IPA) describing the single-particle electronic states and eigenvalues by the Kohn-Sham results (sometimes called random phase approximation (RPA)); the independent-QP approximation using GW results, more precisely eigenvalues in the G_0W_0 scheme, and by solving the BSE to take into account the electron-hole interaction. The resulting spectra versus a wide range of

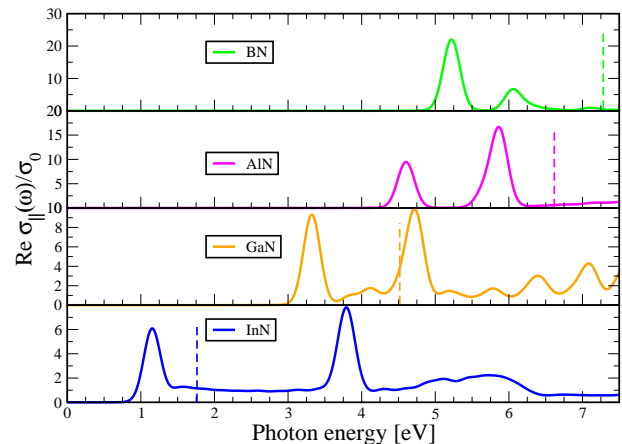


FIG. 2. Real part of the dynamical optical conductivity $Re\sigma_{\parallel}(\omega)$ for in-plane polarization of the 2D nitrides studied. The spectra are normalized to the dc conductivity σ_0 . The direct QP gap is indicated by a vertical dashed line.

In all cases the QP corrections at the G_0W_0 level blueshift the DFT independent-particle spectra without any significant change to their lineshape. The inclusion of $e-h$ interaction through BSE leads to a redshift of absorption spectra and seems to compensate quasiparticle effects, restoring a qualitative agreement with the

position of DFT spectra but not their lineshape (see Figs. SM2 to SM5). Strong peaks appear, due to bound excitons, well below the fundamental direct gaps. However, for GaN and InN, and especially InN, such bound exciton peaks also occur above the fundamental QP gap belonging to high-energy interband transitions and, hence, being resonant with the continuum of scattering states of lower valence-conduction band pairs. The striking difference between the two light polarizations is the significant blueshift of the absorption spectra $\text{Re}\sigma_{\perp}(\omega)$ mainly due to local-field effects described by the electron-hole exchange interaction in the two-particle Hamiltonian $H_{\text{exc}}(2)$ [30, 31]. Thereby, also their intensities are reduced, in particular for BN. In the $\text{Im}\sigma_{\parallel/\perp}(\omega)$ spectra the resonances follow the same trends as for $\text{Re}\sigma_{\parallel/\perp}(\omega)$.

Here, we are mainly interested in excitonic effects at the band edges. For that reason, we focus on the BSE absorption spectra for in-plane light polarization, displayed in Fig. 2. The real part of the in-plane BSE sheet optical conductivity for BN shows the presence of three low-energy peaks of decreasing intensity. For the first exciton at 5.2 eV, usually identified as optical gap E_g^{opt} reduced by the binding energy E_b with respect to the QP gap E_g , we find a large exciton binding energy of 2.0 eV. A second and a weak third peak appear at 6.1 eV and 7.2 eV (see Fig. SM2), respectively. The first structure originates from transitions at the fundamental gap at K between the highest valence band and the lowest conduction band. The second exciton peak has a similar origin (see Fig. SM1). The first two band-edge excitons are related to $\pi \rightarrow \pi^*$ transitions. The third peak belongs mainly to transitions near Γ with some hybridization with σ and σ^* states. Although the position of the peaks is slightly different, our value of the binding energy is in agreement with other predictions [19, 35]. Self-consistency within the GW approximation would blueshift all exciton positions by up to 1 eV and consequently increase E_g^{opt} , at least for BN [35, 36].

The AlN in-plane BSE conductivity exhibits in Fig. 2 two prominent structures of increasing intensity, located at 4.6 eV and 5.9 eV. The binding energy of the first exciton is 1.9 eV. In a previous theoretical work [37] three exciton peaks at 4.12 eV, 4.97 eV and 5.4 eV were found, with a similar binding energy of 1.88 eV. A possible source of discrepancy stems from the lack of the cut in the Coulomb interactions between two sheets in the supercell arrangement in Ref. [37].

Also for GaN we register the presence of two main peaks for the in-plane component of the BSE sheet polarizability near the absorption edge. The first peak appears at 3.3 eV while the second at 4.7 eV, similarly to other calculations [15]. The first exciton presents a large binding energy of 1.2 eV in agreement with Ref. [16] and is mainly due to VBM-CBM transitions near Γ . The second peak has strong contributions of transitions into the second conduction bands at Γ but also of direct transitions near K (see band structure in [13] and in Fig. SM1).

Two bound excitons appear for InN in the BSE optical

conductivity for in-plane light polarization below photon energies of 6 eV. The first exciton, at 1.2 eV, has a binding energy of 0.6 eV and originates VBM-CBM transitions near Γ . A second bound but resonant exciton peak visible at 3.9 eV arises from VBM-CBM transitions near M and K at the BZ boundary.

In all 2D nitrides the first strong excitonic peak originates from transitions at the fundamental direct gap between the highest valence band and the lowest conduction band near Γ (K in the BN case). The corresponding exciton wave functions are plotted in Fig. 3. They repre-

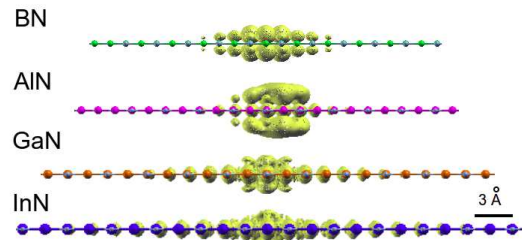


FIG. 3. Exciton wavefunctions for the 2D nitrides: BN; AlN; GaN; InN. In all cases the hole has been fixed near a nitrogen atom (light blue).

sent the probability to find the electron, having fixed the position of the hole near one nitrogen atom. Their localization around the chosen hole position clearly indicates the 2D character of the excitons, which extends above and below the basal plane just for a length of the order of the lattice parameter. The lateral electron-hole distance covers instead a wider range in Fig. 3. By defining the excitonic radius r_{exc} as the first moment

$$r_{\text{exc}} = \int d^3\mathbf{r}_e |\mathbf{r}_e| \psi^*(\mathbf{r}_h, \mathbf{r}_e) \psi(\mathbf{r}_h, \mathbf{r}_e), \quad (7)$$

where $\psi(\mathbf{r}_h, \mathbf{r}_e)$ denotes the exciton eigenstate $|S\mathbf{Q}\rangle$ for the ground state $S = 0$ and $\mathbf{Q} = 0$ in real-space representation, we find an excitonic radius as small as 3.8 Å for 2D BN, and as large as 15.5 Å for 2D InN. Comparing the values r_{exc} in Table II with the lattice constants a in Table I, a clear tendency for the formation of 2D excitons in the ground state from BN to InN becomes visible. The averaged electron-hole distances r_{exc} in BN and AlN are not significantly larger than the lattice parameters. Their lowest energy excitons may be therefore interpreted to possess a Frenkel-like character. Electron and hole in the excitons are found close to nearest-neighbor atoms in the plane with the highest probability. In the case of GaN and InN, however, the larger electron-hole distances r_{exc} suggest a character closer to that of 2D hydrogen-like Wannier-Mott excitons.

The chemical trends of the exciton parameters E_b and r_{exc} in Table II are obvious. They are qualitatively in line with the fundamental QP gaps E_g and the lattice constant a in Table I. As summarized in Fig. 4, with increasing cation atomic number, we find an increasing lattice

	E_g^{opt} (eV)	E_b (eV)	r_{exc} (Å)
BN	5.19	2.0	3.8
AlN	4.60	1.9	4.5
GaN	3.30	1.2	8.0
InN	1.2	0.6	15.5

TABLE II. *Ab-initio* optical gaps E_g^{opt} , excitonic binding energy E_b , and excitonic radius r_{exc} for 2D III-nitrides. All results are derived using the solutions of the BSE (2).

constant, accompanied by a decrease of the QP and optical gaps. The exciton binding energy E_b qualitatively follows the gap energy, which also characterizes the intrinsic screening in the sheet. The electron-hole distance r_{exc} nearly scales with the lattice constant in Table I. A quantitative relationship between the two exciton parameters can be approximately given by $E_b \sim \hbar^2/(2\mu r_{exc}^2)$ with μ as the reduced exciton mass. The prefactor varies between 2.9 and 4.4, thereby indicating that the true *ab-initio* computed excitons are not too far from a 2D

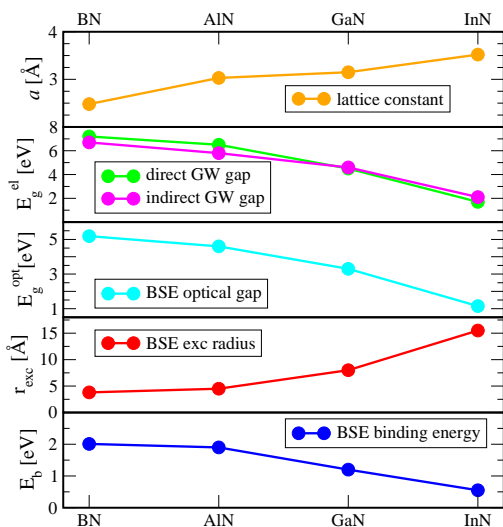


FIG. 4. *Ab-initio* results for the lattice constants, direct and indirect QP gaps, optical gaps, exciton radius, and binding energy of the excitons, for the four 2D materials studied.

C. Model excitons

It is interesting and instructive to compare the *ab-initio* BSE results for exciton binding energy and exciton radius with the prediction of those exciton features obtained using the simple analytic model for excitons in 2D systems [26–28]. The BSE approach, representing at the moment the most elaborated and reliable *ab-initio* method for the inclusion of the excitonic effects, suffers for the heaviness of the calculations. A valid alternative is given by the solution of the eigenvalue problem of the

effective excitonic Hamiltonian (3). This exciton problem can be solved analytically just in the Mott-Wannier limit, i.e., for large electron-hole distances and/or vanishing screening. In fact, for $\rho/2\pi\alpha_{2D} \gg 1$, the unscreened 2D Coulomb potential

$$W(\rho) = -e^2/\rho. \quad (8)$$

appears, and the *e-h* pair feels a bare 2D Coulomb potential. In other words, in the Wannier-Mott limit a 2D exciton is described by an unscreened hydrogen-like model. The eigenvalue problem can be solved analytically [38], resulting in a huge binding energy $E_b = 4R\mu/m$ and a small *e-h* distance $r_{exc} = a_B m/2\mu$ with the hydrogen Rydberg R and the Bohr radius a_B .

In the opposite limit of $\rho/2\pi\alpha_{2D} \ll 1$, i.e., in the limit of small electron-hole distances and/or large sheet polarizabilities, one finds a logarithmic behavior for the screened interaction, namely

$$W(\rho) = \frac{e^2}{2\pi\alpha_{2D}} \left[\ln \left(\frac{4\pi\alpha_{2D}}{\rho} \right) - \gamma \right], \quad (9)$$

where $\gamma = 0.577$ is the Euler constant. In 2D III-N systems, the intermediate range is realized, i.e., neither the Wannier-Mott nor the logarithmic behavior gives a reasonable description. The eigenvalue problem with the full W can be only solved numerically. Since we are mainly interested in the lowest energy excitons, we numerically solve the Schrödinger equation in a variational approach, and get the exciton binding energy E_b^{mod} and radius r_{exc}^{mod} for the first bound $1s$ exciton. The approach requires only the reduced exciton effective mass μ and the sheet polarizability $\alpha_{2D} = L(\text{Re}\epsilon_{\parallel}(\omega=0) - 1)/4\pi$, both easily computed at the DFT level. The inverse of the reduced exciton mass, $1/\mu = 1/m_e + 1/m_h$ is calculated using the effective masses of the electrons and holes reported in Table III.

	α_{2D} (a.u.)	m_h/m_e (m)	E_b^{mod} (eV)	r_{exc}^{mod} (Å)
BN	2.10	0.63/0.96	2.1	3.8
AlN	2.07	1.64/0.59	2.2	3.4
GaN	2.78	0.52/0.26	1.4	6.6
InN	7.76	0.42/0.09	0.5	16.4

TABLE III. Exciton binding energy E_b and excitonic radius r_{exc} for 2D III-nitrides calculated within the 2D excitonic model (3). Also the DFT ingredients α_{2D} and the electron and hole effective masses are reported.

The reliability of the variational method, previously tested on graphene, silicane, and germanane in [27], is demonstrated by comparing the *ab-initio* and 2D model results given in Tables II and III. For both exciton binding energy and exciton radius the chemical trends and the absolute values are in astonishing agreement. The energy deviations are only of the order of 0.1 – 0.2 eV and the radii differences are of the order or less of 20%. For the strongest bound exciton in BN practically the

same values are obtained. The rough description of the ground state of the lowest exciton as a 2D $1s$ variational state

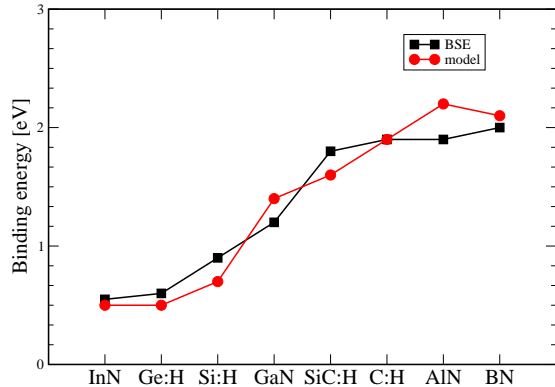


FIG. 5. Comparison of the exciton binding energies calculated *ab-initio* by solving the BSE (black squares), and by solving the 2D excitonic model (red circles).

Analyzing the variational results in Table III we affirm that the model solutions are in good agreement with the results of full *ab-initio* but cumbersome BSE calculations. Although to accurately describe the electron-hole interaction, it is necessary to solve the Bethe-Salpeter equation (2), the model (3) represents a valid alternative to obtain a quick qualitative description of the behavior of lowest energy excitons in 2D materials.

The general validity of this conclusion is underlined in Fig. 5 by the results for the hydrogenated group-IV materials, graphane, silicene-graphane, silicane, and germanane [27, 39, 40], which are in line with the findings for nitride monolayers.

D. Exciton radiative lifetimes

Important material characteristics for light-emitting diodes and laser devices are the rates of different electron-hole recombination processes. Not much is known at the moment about these processes in 2D nitrides. Here, we focus on the exciton radiative lifetimes and compare the results with the corresponding lifetimes of 3D nitrides. Again, we are focused to the lowest-energy excitons $S = 0$ and $\mathbf{Q} = 0$ to find the radiative decay time (5) or its thermal average (6).

Following (5) and (6), we find that the lifetimes $\tau_S(0)$ of BN, AlN, and GaN are very similar to each other, while for 2D InN it is significantly larger (see Table IV). The lifetimes and the exciton binding energies in Table II show opposite trends, in accordance with the Heisenberg uncertainty principle, $\Delta E \Delta t > \hbar$.

The recombination times of the lowest energy excitons, are by more than one order of magnitude smaller than corresponding lifetimes of excitons of transition metal dichalcogenides at the corner points K of the hexagonal BZ [32]. The main reason for this difference is the

	$\tau_S(0)$ (fs)	$\langle \tau_S \rangle$ (ps)	$\langle \tau_S \rangle$ (ns) 3D *
BN	29 (13)	55 (14)	–
AlN	33 (1)	67 (18)	2.4
GaN	35 (18)	73 (36)	3.5/3.8
InN	55 (58)	422 (445)	7.3

TABLE IV. Calculated exciton radiative lifetimes for 2D III-nitrides $\tau_S(0)$ (5) and $\langle \tau_S \rangle$ (6) for room temperature and bound excitons in the ground state $S = 0$ and $\mathbf{Q}=0$. The values in parenthesis have been estimated within the effective mass approximation but *ab-initio* calculated matrix elements (10). The last column lists averaged exciton lifetimes $\langle \tau_S \rangle$ calculated for band-edge excitons of 3D nitrides within the effective-mass approximation [41].

stronger transition matrix elements in the case of the nitrides. Our findings for the radiative lifetimes of the lowest-energy excitons in the 2D nitrides clearly indicate their excellent emission properties. They seem to be more appropriate for LED and laser applications than the transition metal dichalcogenides.

The averaged lifetimes for excitons in the lowest-energy exciton band $\langle \tau_S \rangle$ at room temperature still give rise to shorter lifetimes than the transition metal dichalcogenides [32]. In general, the thermalized excitons in the lowest band $E_S(\mathbf{Q})$ possess an averaged radiative lifetime $\langle \tau_S \rangle$, which is three orders of magnitude larger than $\tau_S(0)$. This is a consequence of the much faster recombination of the excitons with vanishing translational energy. Comparing the averaged lifetimes $\langle \tau_S \rangle$ at room temperature in Table IV with the values for 3D nitrides, differences of one to two orders of magnitude are observed. This fact underlines the outstanding emission properties of 2D nitrides. Due to the quantum confinement, the reduced screening and, hence, the huge exciton binding energies, the sheet crystals made by group-III nitrides appear as ideal materials for active optoelectronic applications.

Finally, for a better understanding of the exciton radiative decay rates, we also apply the variational solutions for the lowest $1s$ excitons with a pure 2D screening derived in Ref. [27]. Within this model the exciton dipole matrix elements may be replaced by

$$\mu_S^2 = \frac{\hbar^2}{m^2 E_S^2(0)} |\langle v\mathbf{k} | p_{\parallel} | c\mathbf{k} \rangle|^2 A_{uc} \Phi_{S0}^2(0) \quad (10)$$

with the momentum matrix element $\langle v\mathbf{k} | p_{\parallel} | c\mathbf{k} \rangle$ taken at the BZ center $\mathbf{k}=0$ (or at a corner point K of the BZ in the case of BN). For vanishing electron-hole distance the $1s$ exciton wavefunction for the internal motion $\Phi_{S0}(0) = (\frac{2}{\pi r_{exc}^2})^{1/2}$ is simply determined by the inverse exciton radius r_{exc} . With the parameters summarized in Table II we find the values given in parenthesis in columns 1 and 2 of Table IV. They are close to those computed *ab-initio*. These findings indicate that the material dependence, the chemical trend, can be described by $\tau_S(0) \sim E_g^{opt} r_{exc}^2 / |\langle v\mathbf{k} | p_{\parallel} | c\mathbf{k} \rangle|^2$. For the thermally averaged quantities it holds $\langle \tau_S \rangle \sim \tau_S(0) M / (E_g^{opt})^2$. These

relations are in qualitative agreement with the variation of the *ab-initio* exciton lifetimes with the 2D crystal discussed above. However, Fig. 6 also clearly indicates that the material dependence on the optical matrix element square $|\langle v\mathbf{k} | p_{\parallel} | c\mathbf{k} \rangle|^2$ is not negligible, at least going from GaN to InN. Along the row BN, AlN and GaN, this dependence is weak.

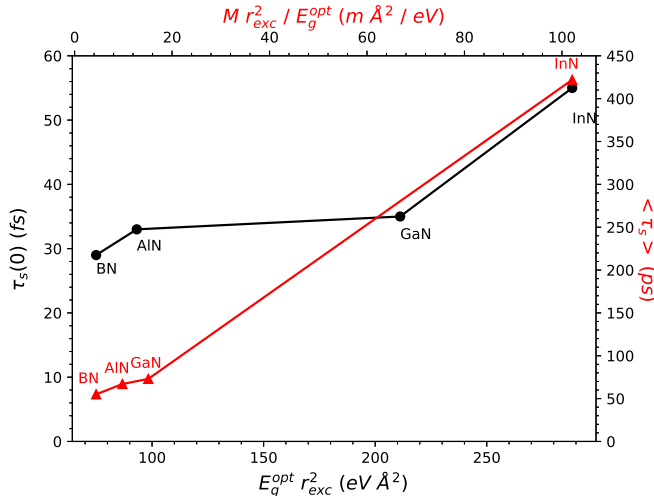


FIG. 6. Excitonic lifetimes $\tau_S(0)$ and $\langle \tau_S \rangle$ at 300 K of the 2D nitrides versus characteristic exciton parameters.

IV. CONCLUSIONS

The excitonic properties of electron-hole-pair excitations below the absorption edge are investigated *ab-initio* for group-III nitride monolayers. The quasiparticle electronic structure is computed within the G_0W_0 approximation in a perturbation-theory manner starting from the optimized atomic geometries and the Kohn-Sham eigenvalues and eigenfunctions. The two-particle excitations and the accompanying optical properties are predicted by solving the Bethe-Salpeter equation with screened electron-hole attraction and electron-hole exchange. In addition to the absorption of the lowest bound electron-hole pairs, their emission properties are also studied by computing the exciton radiative lifetimes. In order to characterize the motion of electrons and holes

forming the excitons, the characteristic exciton parameters, as appearing for these pair excitations in both absorption and emission, are also investigated in a variational framework by applying static sheet polarizabilities to describe the screening and the effective mass approximation. *Ab-initio* and model excitonic parameters are compared.

We have demonstrated a significant influence of the electron-hole interactions on the optical spectra of the 2D nitrides, in particular on the absorption spectra. Strong bound exciton peaks appear below the direct quasiparticle gap. The lowest energy excitons exhibits huge exciton binding energies of 0.6 – 2.0 eV going from InN to BN. These pair excitations are almost two-dimensional. Their wavefunctions are localized in the plane of the 2D nitrides. Thereby, the average electron-hole distances vary between 3.8 and 15.5 Å from BN to InN, indicating a transition from a Frenkel-like to a Wannier-Mott-like behavior along the row BN, AlN, GaN, and InN. Indeed, these lowest-energy excitons can be qualitatively described within the effective mass approximation for the kinetic energy of electrons and holes and a screened Coulomb potential in the sheet plane with a weak screening due to the 2D static electronic polarizability. The variational results for binding energy and exciton radius illustrate the almost 2D 1s-like character of the wavefunction describing the internal exciton motion.

The emission properties of the 2D nitrides are illustrated by the radiative lifetimes of the lowest-energy excitons. We observed lifetimes of the order of 30 – 60 fs, much faster than for other 2D semiconductors. In the case of the thermal average of these excitons with finite translation vector in the lowest exciton band, the radiative lifetimes increase substantially. However, their low values indicate that group-III nitride sheets appear to be promising materials for active optoelectronic applications in the visible up to the vacuum ultraviolet region. Hetero-combinations of such 2D nitrides, e.g. of InN and GaN, may be also applied in efficient photovoltaic devices.

V. ACKNOWLEDGMENTS

O.P. and I.K. acknowledge financial support from the EU MSCA HORIZON2020 project 'CoExAN' (GA644076). CPU time was granted by CINECA HPC center. We thank Valerio Olevano for useful discussions.

[1] Q. H. Wang, K. Kalantar-Zadeh, A. Kis, J. N. Coleman, and M. S. Strano, *Nat Nano* **7**, 699 (2012).
 [2] S. Balendhran, S. Walia, H. Nili, S. Sriram, and M. Bhaskaran, *Small* **11**, 640 (2015).
 [3] F. Xia, H. Wang, D. Xiao, M. Dubey, and A. Ramasubramanian, *Nature Photonics* **8**, 899 (2014).
 [4] C. Grazianetti, S. De Rosa, C. Martella, P. Targa, D. Codegioni, P. Gori, O. Pulci, A. Molle, and S. Lupi,

Nano letters **18**, 7124 (2018).

[5] S. Nakamura, *Rev. Mod. Phys.* **87**, 1139 (2015).
 [6] A. Nagashima, N. Tejima, Y. Gamou, T. Kawai, and C. Oshima, *Physical Review Letters* **75**, 3918 (1995).
 [7] P. Tsipas, S. Kassavetis, D. Tsoutsou, E. Xenogiannopoulou, E. Golias, S. Giamini, C. Grazianetti, D. Chiappe, A. Molle, M. Fanciulli, *et al.*, *Applied Physics Letters* **103**, 251605 (2013).

- [8] S. Alamé, A. N. Quezada, D. Skuridina, C. Reich, D. Henning, M. Frentrup, T. Wernicke, I. Koslow, M. Kneissl, N. Esser, *et al.*, *Materials Science in Semiconductor Processing* **55**, 7 (2016).
- [9] Z. Y. Al Balushi, K. Wang, R. K. Ghosh, R. A. Vilá, S. M. Eichfeld, J. D. Caldwell, X. Qin, Y.-C. Lin, P. A. DeSario, G. Stone, *et al.*, *Nature materials* **15**, 1166 (2016).
- [10] D. Kecik, A. Onen, M. Konuk, E. Gürbüç, F. Ersan, S. Cahangirov, E. Aktürk, E. Durgun, and S. Ciraci, *Applied Physics Reviews*, *Applied Physics Reviews* **5**, 011105 (2018).
- [11] H. Sahin, S. Cahangirov, M. Topsakal, E. Bekaroglu, E. Akturk, R. T. Senger, and S. Ciraci, *Phys. Rev. B* **80**, 155453 (2009).
- [12] A. Onen, D. Kecik, E. Durgun, and S. Ciraci, *Phys. Rev. B* **93**, 085431 (2016).
- [13] M. S. Prete, A. Mosca Conte, P. Gori, F. Bechstedt, and O. Pulci, *Applied Physics Letters* **110**, 012103 (2017).
- [14] V. Wang, Z. Q. Wu, Y. Kawazoe, and W. T. Geng, *The Journal of Physical Chemistry C*, *J. Phys. Chem. C* **122**, 6930 (2018).
- [15] H. Shu, X. Niu, X. Ding, and Y. Wang, *Applied Surface Science* **479**, 475 (2019).
- [16] N. Sanders, D. Bayerl, G. Shi, K. A. Mengle, and E. Kioupakis, *Nano letters* **17**, 7345 (2017).
- [17] D. Liang, R. Quhe, Y. Chen, L. Wu, Q. Wang, P. Guan, S. Wang, and P. Lu, *RSC Adv.* **7**, 42455 (2017).
- [18] M. S. Prete, O. Pulci, and F. Bechstedt, *Phys. Rev. B* **98**, 235431 (2018).
- [19] L. Wirtz, A. Marini, and A. Rubio, *Physical Review Letters* **96**, 126104 (2006).
- [20] W. Kohn and L. J. Sham, *Physical review* **140**, A1133 (1965).
- [21] P. Giannozzi, S. Baroni, N. Bonini, M. Calandra, R. Car, C. Cavazzoni, D. Ceresoli, G. L. Chiarotti, M. Cococcioni, I. Dabo, *et al.*, *Journal of physics: Condensed matter* **21**, 395502 (2009).
- [22] P. Giannozzi, O. Andreussi, T. Brumme, O. Bunau, M. B. Nardelli, M. Calandra, R. Car, C. Cavazzoni, D. Ceresoli, M. Cococcioni, *et al.*, *Journal of Physics: Condensed Matter* **29**, 465901 (2017).
- [23] F. Bechstedt, *Many-Body Approach to Electronic Excitations* (Springer, 2016).
- [24] See www.etsf.eu for the GW code CHISIG developed within the ETSF.
- [25] <http://etsf.polytechnique.fr/exc>.
- [26] P. Cudazzo, I. V. Tokatly, and A. Rubio, *Physical Review B* **84**, 085406 (2011).
- [27] O. Pulci, M. Marsili, V. Garbuio, P. Gori, I. Kupchak, and F. Bechstedt, *Physica Status Solidi (b)* **252**, 72 (2015).
- [28] L. Keldysh, *JETP Letters* **29**, 658 (1979).
- [29] R. Guseinov, *Physica Status Solidi (b)* **125**, 237 (1984).
- [30] L. Matthes, O. Pulci, and F. Bechstedt, *Physical Review B* **94**, 205408 (2016).
- [31] G. Moody, J. Schaibley, and X. Xu, *JOSA B* **33**, C39 (2016).
- [32] M. Palummo, M. Bernardi, and J. C. Grossman, *Nano letters* **15**, 2794 (2015).
- [33] S. Cahangirov, M. Topsakal, E. Aktürk, H. Şahin, and S. Ciraci, *Physical review letters* **102**, 236804 (2009).
- [34] L. C. de Carvalho, A. Schleife, and F. Bechstedt, *Phys. Rev. B* **84**, 195105 (2011).
- [35] I. Guilhorn, *Phys. Rev. B* ((resubmitted)).
- [36] N. Berseneva, A. Gulans, A. V. Krasheninnikov, and R. M. Nieminen, *Phys. Rev. B* **87**, 035404 (2013).
- [37] C. Bacaksiz, A. Dominguez, A. Rubio, R. T. Senger, and H. Sahin, *Physical Review B* **95**, 075423 (2017).
- [38] H. Haug and S. Koch, *Quantum Theory of the Optical and Electronic Properties of Semiconductors* (World Scientific, Singapore, 2009).
- [39] O. Pulci, P. Gori, M. Marsili, V. Garbuio, R. D. Sole, and F. Bechstedt, *EPL (Europhysics Letters)* **98**, 37004 (2012).
- [40] P. Gori, O. Pulci, M. Marsili, and F. Bechstedt, *Applied Physics Letters* **100**, 043110 (2012).
- [41] A. Dmitriev and A. Oruzhenikov, *Journal of applied physics* **86**, 3241 (1999).

SUPPLEMENTAL MATERIAL: Excitonic effects in absorption and emission of 2D group-III nitrides

M.S. Prete, D. Grassano,* and O. Pulci
*Department of Physics, and INFN, University of Rome Tor Vergata,
Via della Ricerca Scientifica 1, I-00133 Rome, Italy*

Ihor Kupchak
*V.E. Lashkaryov Institute of Semiconductor Physics,
National Academy of Sciences of Ukraine, Kyiv, Ukraine*

Friedhelm Bechstedt
Institut für Festkörperteorie und -optik, Friedrich Schiller Universität, Max-Wien-Platz 1, 07743 Jena, Germany
(Dated: December 15, 2024)

I. QUASIPARTICLE ELECTRONIC STRUCTURE

The electronic band structures of the 2D group-III nitrides are displayed in Fig. SM1. Although their geometry resembles that of the graphene, the different electronegativities between nitrogen and B, Al, Ga and In atoms open significant gaps at the K points of the Brillouin zone (BZ). The conduction band minimum moves to the Γ point for all materials studied. In the case of the light cation, i.e., BN and AlN, the valence band maximum is fixed at K (as in graphene). However, in the case of the heavier cations, Ga and In, it also moves to the Γ point.

Direct allowed optical transitions are indicated in Fig. SM1 by vertical arrows for not too large interband energies. The lowest one occurs at Γ , independent of the cation. Higher-energy transitions are however possible at M and K between the uppermost valence band and the lowest conduction band. Transitions into the second-lowest conduction band may also occur at Γ , in particular for BN and AlN, where the energy distance to the conduction band minimum is relatively small compared to the gap size.

II. OPTICAL SPECTRA

In order to characterize the linear optical properties of the monolayer nitrides, the real and imaginary parts of the 2D optical conductivity are presented in Figs. SM2 – SM5 for both in-plane and out-of-plane light polarization. The many-body effects are described in three different approximations:

- (i) In the independent-particle approximation the electron-hole interactions are not taken into account. The single-particle eigenfunctions and eigenenergies are taken from the Kohn-Sham (KS) approach.
- (ii) In the independent-quasiparticle (QP) approach the KS eigenvalues are corrected by QP shifts computed within the G_0W_0 approximation for exchange and correlation interactions. Correspondingly, the spectra are significantly blueshifted by about 2.5 eV (BN, AlN), 1.8 eV (GaN), and 1.0 eV (InN).
- (iii) The BSE spectra including the screened electron-hole attraction and the unscreened electron-hole exchange interaction are characterized by three important features with respect to the independent-QP approach. There is, in general, a redshift accompanied by a spectral redistribution. The most striking feature is, however, the formation of bound exciton states below the QP gaps.

These phenomena are visible in the real parts or the optical conductivity, especially by significant peaks, while in its imaginary parts still some resonance features are observable. The real parts vanish for small photon energies. Their slopes characterize the dielectric properties of the sheets.

The most important feature of changing the light polarization from an in-plane position to the (normal) out-of-plane direction is a significant blueshift of the spectra. It can be related to depolarization effects or local-field effects as described by the electron-hole exchange interaction in the pair Hamiltonian H_{exc} .

* davide.grassano@roma2.infn.it

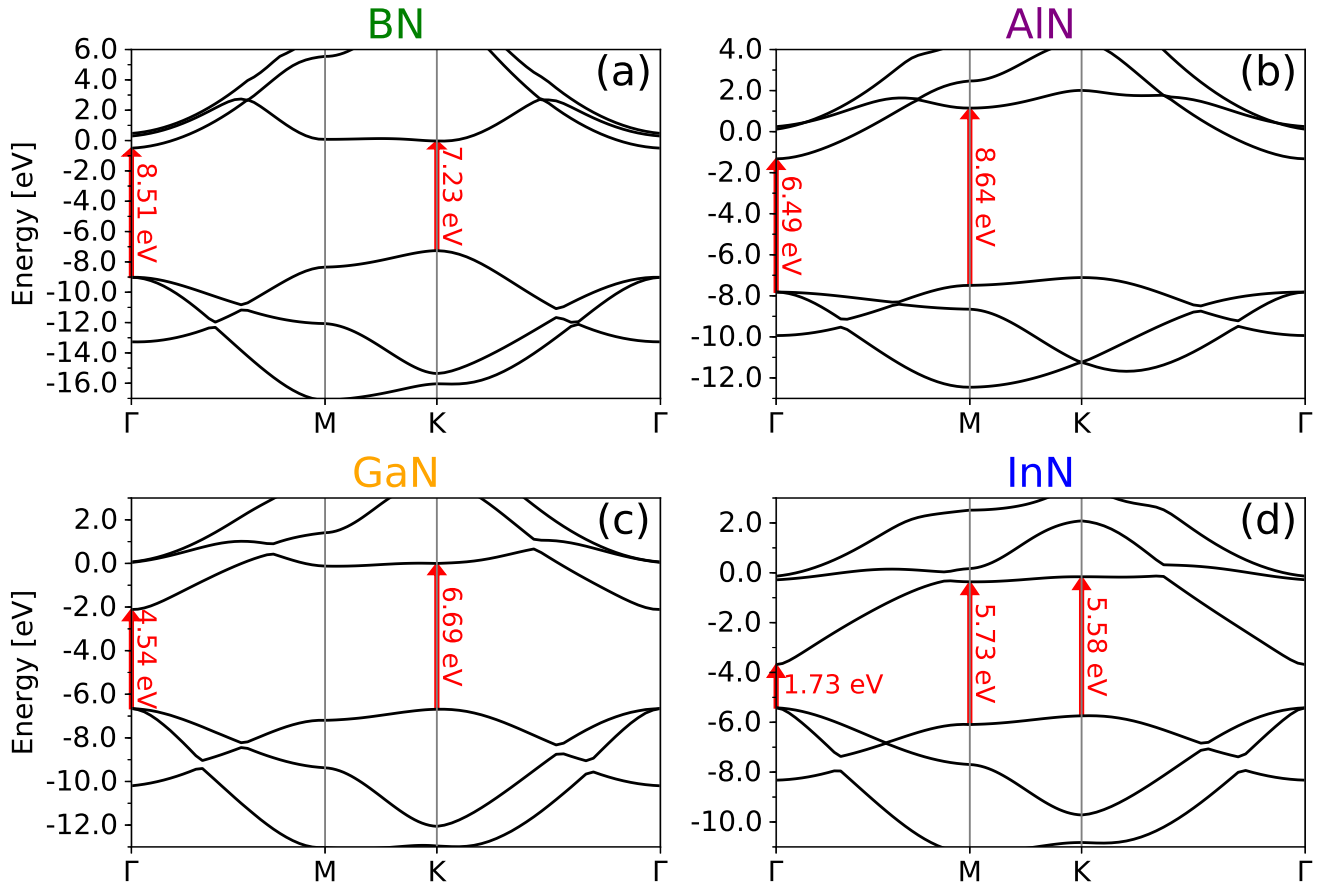


FIG. SM1. Electronic quasiparticle band structures of (a) BN, (b) AlN, (c) GaN and (d) InN sheet crystals obtained within the one-shot G_0W_0 approximation. The vertical arrows indicate possible strong optical transitions in these 2D materials. The vacuum level position is used as energy zero.

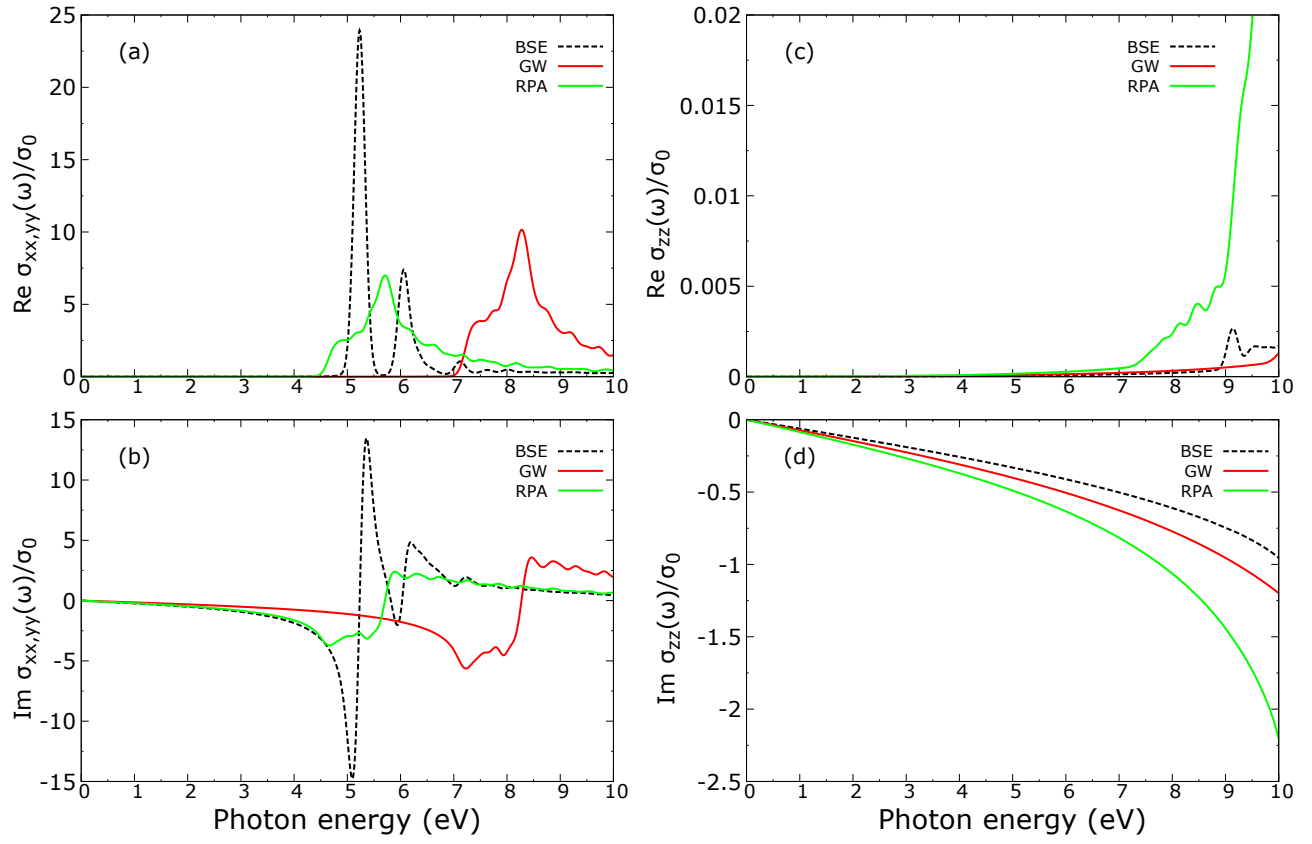


FIG. SM2. Real (a,c) and imaginary (b,d) parts of optical conductivity for BN calculated within the independent-particle approach (RPA - green lines), within the independent-quasiparticle approach (GW - red lines) and taking into account excitonic effects (BSE - black dotted lines) for in-plane (a,b) and out-of-plane polarization (c,d).

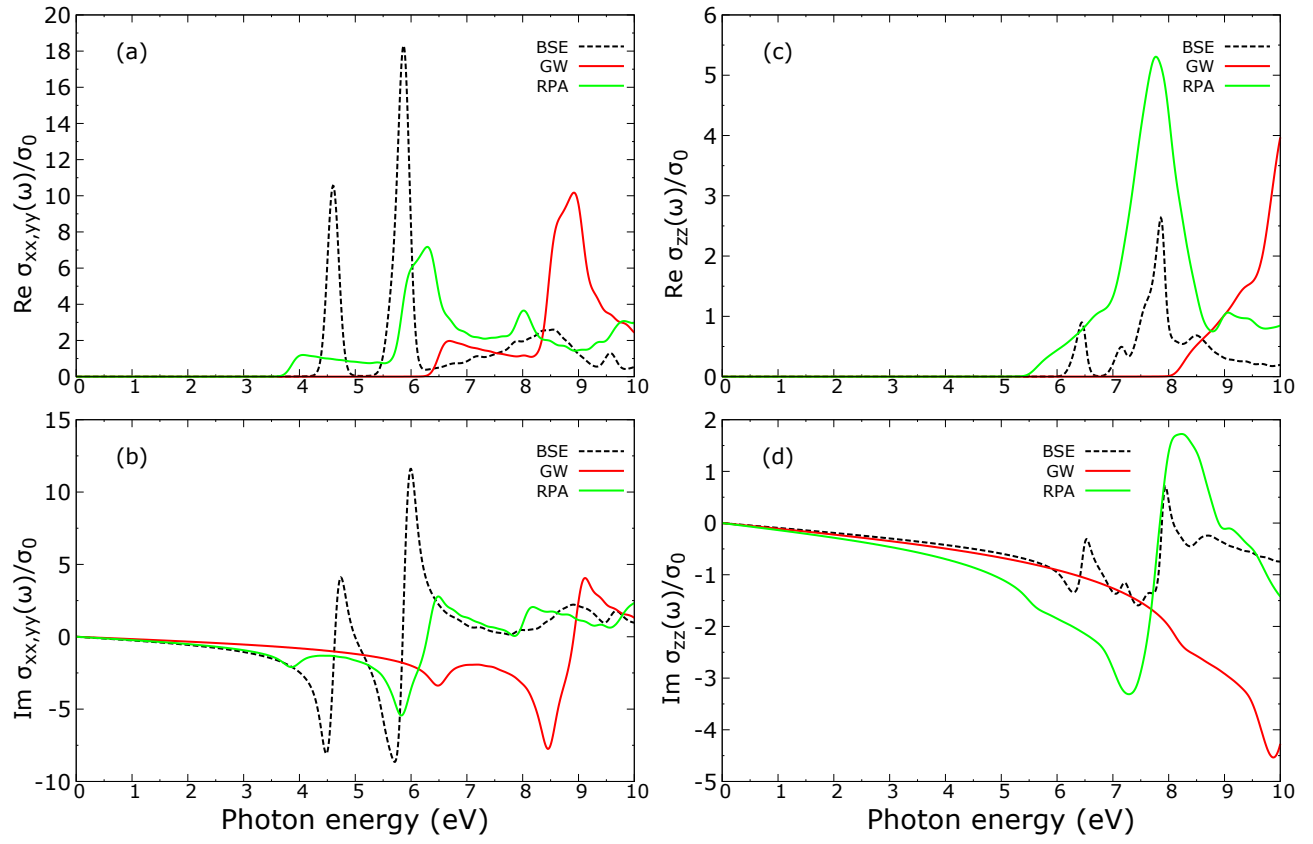


FIG. SM3. Real (a,c) and imaginary (b,d) of optical conductivity for AlN calculated within the independent-particle approach (RPA - green lines), within the independent quasiparticle approach (GW - red lines) and taking into account excitonic effects (BSE - black dotted lines) for in-plane (a,b) and out-of-plane polarization (c,d).

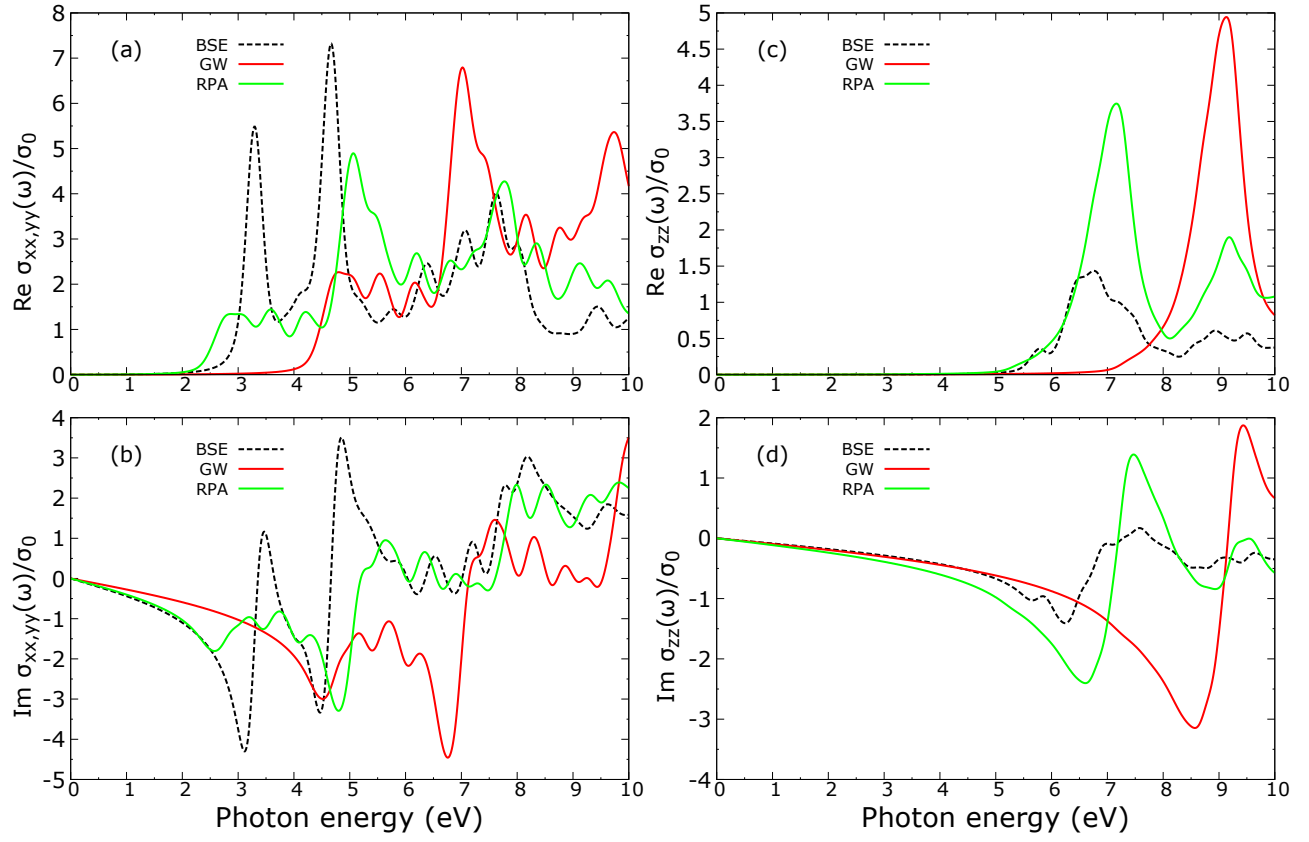


FIG. SM4. Real (a,c) and imaginary (b,d) of optical conductivity for GaN calculated within the independent-particle approach (RPA - green lines), within the independent quasiparticle-approach (GW - red lines) and taking into account excitonic effects (BSE - black dotted lines) for in-plane (a,b) and out-of-plane polarization (c,d).

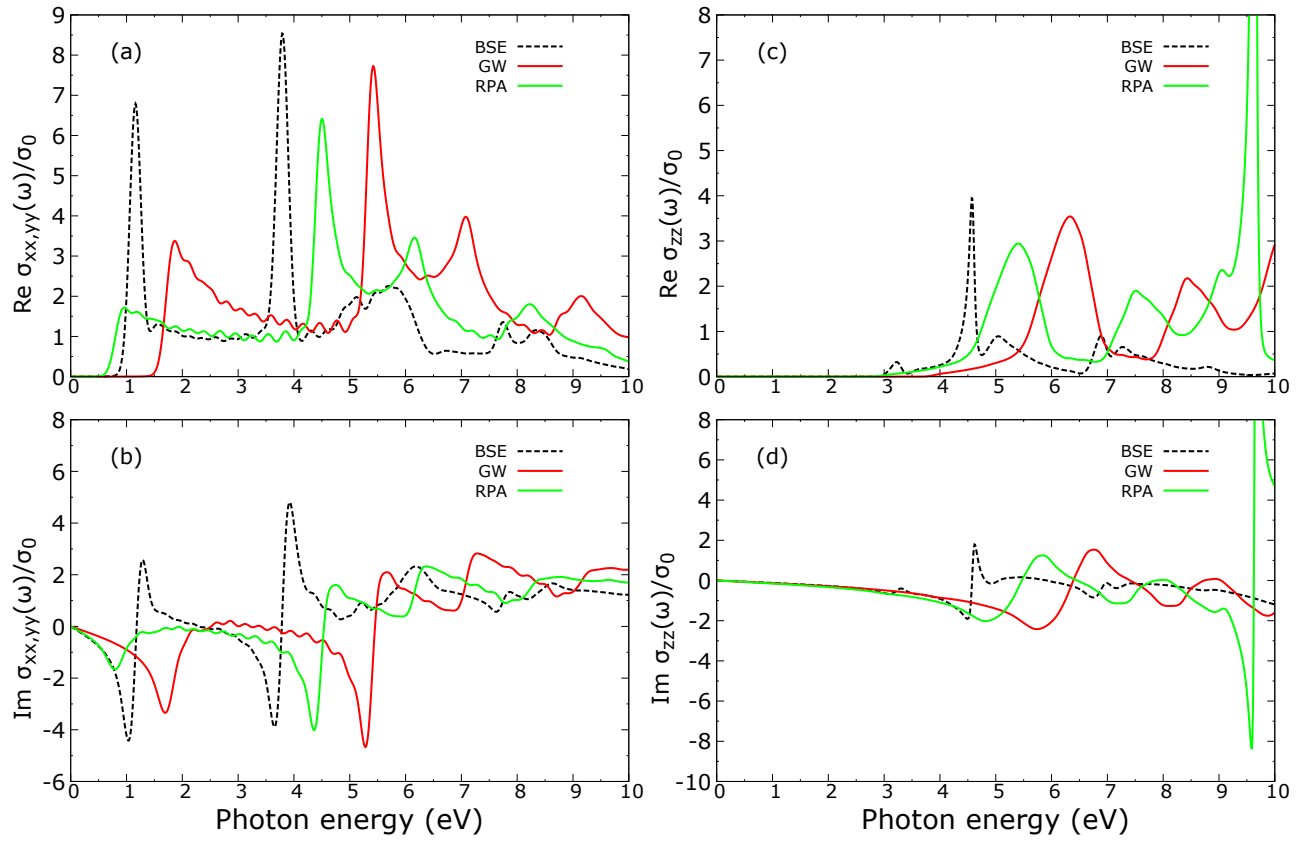


FIG. SM5. Real (a,c) and imaginary (b,d) of optical conductivity for InN calculated within the independent-particle approach (RPA - green lines), within the independent quasiparticle-approach (GW - red lines) and taking into account excitonic effects (BSE - black dotted lines) for in-plane (a,b) and out-of-plane polarization (c,d).